Chinese Journal of Physics 73 (2021) 462–478

Contents lists available at ScienceDirect

Chinese Journal of Physics

journal homepage: www.sciencedirect.com/journal/chinese-journal-of-physics

Simultaneous features of Wu's slip, nonlinear thermal radiation and activation energy in unsteady bio-convective flow of Maxwell nanofluid configured by a stretching cylinder

Yun-Xiang Li [a], Hassan Waqas [b], Kamel Al-Khaled [c], Shan Ali Khan [b], M. Ijaz Khan [d,e], Sami Ullah Khan [f], Rabia Naseem [b], Yu-Ming Chu [g,*]

[a] School of Science, Hunan City University, Yiyang 413000, P. R. China
[b] Department of Mathematics, Government College University Faisalabad, Layyah Campus, 31200, Pakistan
[c] Department of Mathematics & Statistics, Jordan University of Science and Technology, P.O. Box 3030, Irbid 22110, Jordan
[d] Department of Mathematics, Riphah International Universtity, I-14, Islamabad 44000, Pakistan
[e] Nonlinear Analysis and Applied Mathematics (NAAM)-Research Group, Department of Mathematics, Faculty of Sciences, King Abdulaziz University, P.O. Box 80203, Jeddah 21589, Saudi Arabia
[f] Department of Mathematics, COMSATS University Islamabad, Sahiwal 57000, Pakistan
[g] Department of Mathematics, Huzhou University, Huzhou 313000, PR China

ARTICLE INFO

Keywords:
Bioconvection flow
Stretching cylinder
Maxwell nanofluid
Higher order slip
Shooting scheme

ABSTRACT

This continuation deals with the bioconvection flow of magnetized Maxwell nanofluid over a stretched cylinder in presence of slip effects. The novel features of activation energy and thermal radiation are also encountered to analyze the flow. The higher order slip relations are introduced to inspect the thermal flow problem. The flow model is developed in terms of dimensionless equations via appropriate variables. The numerical simulations are presented with shooting scheme by using MATLAB software. The physical outcomes of interesting parameters are visualized. The observations show that velocity profile reduces with unsteady parameter, curvature constant and second order slip factor. The temperature profile enhanced with first order velocity slip parameter and curvature constant. Moreover, nanofluid concentration reduces with Lewis number and Brownian constant.

1. Introduction

The nanofluids are suspension of solid nanoparticles into the base materials, which show great potential in thermal engineering and many industrial applications. With enhanced thermal efficiencies, the nanofluids present many valuable applications in energy production, microelectronics cooling system, microelectronics, extrusion systems, air conditioning, chemical processes, solar systems, refrigeration systems etc. The nanofluids are combination of smaller nanoparticles with base fluids. The presence of nano solid materials in traditional fluids has improved heat transformation properties. It is emphasized that the thermal conductivity of nanoparticles is increased by volume fraction, particulates size, heat, including thermal conductivity. Nanotechnology is of great significance in several industries, such as chemicals and metallurgical machinery, transport, macroscopic objects, cancer treatment, electricity production, respectively. Nanofluids are the mixtures of nanometer-sized particulate suspensions with traditional fluids, the

* Corresponding author.
E-mail address: chuyuming@zjhu.edu.cn (Y.-M. Chu).

https://doi.org/10.1016/j.cjph.2021.07.033
Received 9 December 2020; Received in revised form 13 June 2021; Accepted 20 July 2021
Available online 4 August 2021

first of which was introduced by Choi [1]. Buongiorno [2] discusses the two unusual slipping mechanisms particularly Brownian diffusion and thermophoresis motion effect to increase the natural convection rate of heat energy distribution. Venkatadri et al. [3] experimented the Melting heat exchange of an electrical conductor flow of nanofluid against an exponentially shrinking / expanded porous layer with nonlinear Radiative Cattaneo Christov heat flux under a magnetic field. Mondalet al. [4] studied the influence of the heat exchange of Magnetohydrodynamic on stagnation point nanoliquid flow across an extending or declining surface through homogeneous chemical processes. Yinget al. [5] investigated the Radiative heat transmissions of molten salt-based nanoliquid over cooling coil through the non-uniform heat flux. Waqas et al. [6] inspected the MHD flow of Oldroyd-B nanofluid analytically in presence of magnetic force. Eid et al. [7] described the modification of thermal conductivity including heat transfer impacts on the magneto-water nanofluid flowing in a porous channel with slipping condition. Numerous researchers are interested on nanofluid investigation with Buongiorno modal seen refs. [8-12]. Kamal et al. [13] studied analytically the characteristics of the viscoelastic copper nanofluid with doubled diffusion problem created by 3-D flowing of stagnation point produced by the heat production under the space environment. Anuaret al. [14] analyzed the Maxwell nanofluids thermo Radiative stagnation point flowing over inconsistent convectively warmed stretching surface. Rizwanaet al. [15] investigated on the oblique stagnation point flowing of produced magnet field acrossthe oscillatory surface for non-Newtonian liquid. Giri et al. [16] outlined the process of melting heat transfer in Magnetohydrodynamic nanofluid flowing between two horizontal constructed plates in a revolving structure. Mahanthesh et al. [17] addressed numerically the thermal perspective of MoS_2–Ag hybrid nanoparticles over a wedge. Akram et al. [18] addressed the thermal applications of silver-water based nanoparticles for asymmetric flow. Narla et al. [19] inspected the electro-osmotic applications of nanofluids in a curved microchannel. Akbar et al. [20] intedned the impact of magnetic induction for ciliary-induced flow of Cu-H_2O nanofluids. The numerical simulations based on the successive linearization scheme for the magnetized flow of nanofluid were visualized by Shahid et al. [21]. Akbar et al. [22] addressed the modified diffusion flow of nanofluid with injection and suction applications. Nayak et al. [23] identified the radiation features for the nanofluid flow with magnetic force impact numerically.

The analysis of the mass transport mechanism subject to the chemical process system has attracted significant attention of investigators due to its useful applications in geothermal technologies, mechano-chemicals, nuclear plant chilling, substance destruction, water and oil emulsification etc. These mechanisms include the Arrhenius activation energy along with the binary chemical mechanism of the organisms. Frequently, the relation of chemical substances to mass transport is much complicated and can be continuously studied by digestion and manufacture of reactant material at different rates for mass transport and fluid flowing. In the past, the concept of mass transport was illustrated without taking into consideration the characteristic of Arrhenius energy activation. Activation energy is the minimum amounts of energy required to initiate the chemical reaction. The Swedish mathematician Syante Arrhenius in 1889 was introduced the term of activation energy [24]. There are numerous publications of activation energy in the fluid mechanics that describe the physical characteristics of the pre-exponential component including the chemical process. The phenomenon of energy activation is very important in a several area, including oil tank measuring, oil emulsification and water engineering. Firstly, Bestman [25] identified a mass transformation mechanism including specific properties. Salahuddin et al. [26] investigated the steady-state 3-D velocity and internal energy modification in moving viscoelastic fluid motion along convective conditions on starching surface. Khan et al. [27] described the influence of the heat and mass flux model to the convective flow of Walter-B nanoliquid across a stretching surface with Joule heat concept. Khan et al. [28] scrutinized the Entropy generation configuration in the movement of non-Newtonian nanoparticles with binary chemical processes including activation energy via extending sheet.

The mechanism of bioconvection can be described as the up swimming of the microorganisms in substances that are less dense than water. Owing to the higher accumulation of microorganisms, the above layer of the substances appears too dense and fragile, which induces the microorganisms to break down, due to bioconvection flow. Such microorganisms are including gravitaxis (gravity acceleration), gyrotaxis, and oxytaxis (lower part-heavy) organisms. The two prominent characteristics of organisms displaying bioconvection involve like higher thickness as compared to water and separated individuals swimming forward onto averages. Microorganisms, several of which are the older organisms in the globe identified to human being, are very significant in numerous aspects. It is identified as the method of development in substances of microorganisms, like bacteria or algae, owing to the up-swimming microorganism. Bioconvection has numerous applications in the area of biochemistry and bioengineering. In diesel fuel products, bioreactors and fuel cell engineering, the bioconvection mechanism is used by biomedical engineering. Platt [29] was the firstly person to identify the phenomena of bioconvection. He introduced the unbalanced distributions of density as a procedure for structure establishing in suspensions of swim motile microorganisms and developed the word bioconvection. The term of nanofluids bioconvection was possibly presented firstly by Kuznetsov [30]. Kuznetsov [31] subsequently developed this concept and focusing on nanofluids including gyrotactic motile microorganisms, indicating that the resulting large-scale movement of fluid induced by self-propelled motile gyrotactic microorganisms improves mixture and removes nano-materials accumulation in nanofluids. Haq et al. [32] analyzed the flow characteristics of Cross nano-materials across extended surfaces subjected to Arrhenius activation energy and magnetization field. Ahmad et al. [33] investigated of the bioconvection nanofluid flow containing gyrotactic motile microorganisms with a chemical reaction allowance through a porous medium past a stretched surface. Elanchezhian et al. [34] worked on the rate of motile gyrotactic microorganisms in the Oldroyd-B bio-convective nanofluid flow past a stretched surface with mix convective and inclination magnetization field. Bhatti et al. [35] processed a mathematical study on migration motile swimming microorganisms in the non-Newtonian blood-based nanoliquid through anisotropic restricting artery. Khan et al. [36] outlined the important rheological characteristics of Jeffrey's gyrotactic motile microorganism-including nanofluid across an accelerating formation. Shafiq et al. [37] evaluated of the rate of heat and mass transformation containing gyrotactic micro-organisms with second grade nanofluid flow. Kotnurkaret al. [38] discussed the bioconvection swimming 3rd-grade nanoliquid flowing consisting motile organisms via Copper-blood nanofluids in porous walls. Muhammad et al. [39] recognized the time-dependent movement of magnetization

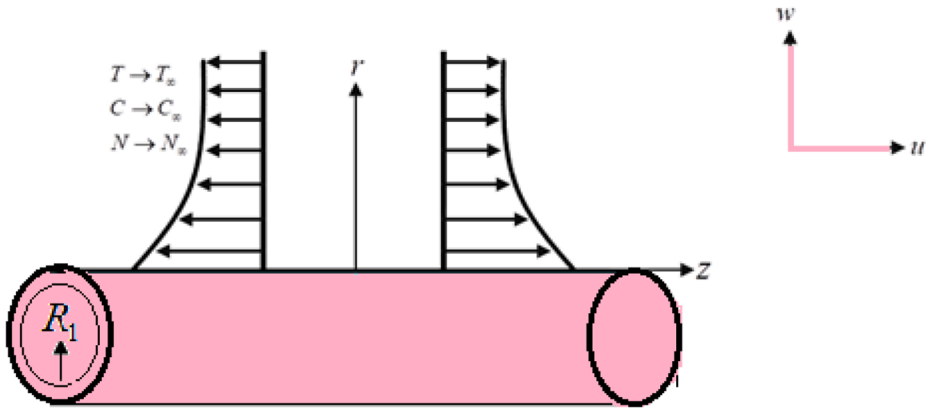

$$u(t,z,r) = u(t,z) + \mathrm{U}_{slip} = \frac{az}{1-\gamma t} + \mathrm{U}_{slip}, w(t,z,r) = 0, -k\frac{\partial T}{\partial r} = h_f\left(T_f - T\right)$$

$$D_B\frac{\partial C}{\partial r} + \frac{D_T}{T_\infty}\frac{\partial T}{\partial r} = 0, \mathrm{N} = \mathrm{N}_w, \qquad at\ r = R_1,$$

Fig. 1. Flow pattern of the problem.

thermophysical Carreau nanofluids conveying motile microorganisms across a rotating wedge through velocity slip as well as thermal radiation characteristics. Farooq et al. [40] introduced an entropic illustration of the 3-D bioconvective flowing of nanoliquid throughout a linearly rotating plate in the absence of magnetic impacts. Hosseinzadehet al. [41] explored the cross-fluid flowing of motile microorganisms and nano-materials throughout a 3-D stretching cylinder. Kairi et al. [42] pointed out the thermosolutal Marangoni features in the bioconvection transport of nanofluids over inclined surface. Shaw et al. [43] addressed the viscous dissipation and magnetic force impact for the nanofluid flow with gyrotactic microorganisms due to permeable sphere. Magagula et al. [44] presented a double dispersed nanofluid model over stretched surface with bioconvection significances. Shaw et al. [45] explained the interpretation of Soret features for nanofluid flow n porous space with uniform suspension of microorganisms.

Following to the interesting applications of nanofluids and bioconvection, current analysis presents the unsteady flow of Maxwell nanofluid containing microorganisms over a stretched cylinder. The novel thermal aspects of nonlinear thermal radiation, activation energy and magnetic features are also introduced. Unlike to the traditional attempts, the analysis is inspected by using the higher order slip relations. The motivations for considering the higher order slip relations are justified as it results two slip parameters which control the velocity but improve the heat and mass transportation rate. The relaxation features are successfully predicted by using the Maxwell fluid model [46, 47]. The Maxwell nanofluid contains gyrotactic microorganisms which help to improve the stability of non-Newtonian nano-materials. It is emphasized that some studies are already available in the literature regarding the bioconvection flow of Maxwell nanofluid over stretched surface however; the bioconvection thermal model with these flow features is not reported yet. This research aims to fulfill this research gap. The highly nonlinear coupled equations are numerically evaluated with shooting technique. Physical consequences is observed for each flow parameter again velocity, nanofluid temperature, concentration and microorganism profile.

2. Mathematical formulation

This model appraises a two-dimensional and bioconvection flow of Maxwell nanofluid containing gyrotactic microorganisms over an expanding cylinder having radius R_1. The activation energy and magnetic field features also utilized in the nanofluid modal. The velocity of cylinder along z-direction is denoted with $u(t,z) = \frac{az}{1-\gamma t}$ where $a = \frac{U_0}{L}$ is the stretching rate. Moreover, γ is the positive constant with property $\gamma t \leq 1$. The polar coordinates of the stretched cylinder are defined as (z,r) . Here, the $z-axis$ is taken along the cylinder while $r-axis$is perpendicular to the cylindrical surface as shown in Fig. 1. In addition, the heat source/sink relations are also introduced in heat equation. The nanofluid temperature is symbolized with T. Moreover, the motile density and concentration of nanofluid is represented with C and N, respectively.

The governing equations for bio-convective transport of Maxwell nanofluid are expressed [46, 47]:

$$\frac{\partial(ru)}{\partial z} + \frac{\partial(rw)}{\partial r} = 0, \tag{1}$$

$$\frac{\partial u}{\partial t}+u\frac{\partial u}{\partial z}+w\frac{\partial u}{\partial r}+\lambda_1\left[\frac{\partial^2 u}{\partial t^2}+2u\frac{\partial^2 u}{\partial t\partial z}+2w\frac{\partial^2 u}{\partial r\partial t}+u^2\frac{\partial^2 u}{\partial z^2}+2uw\frac{\partial^2 u}{\partial r\partial z}+w^2\frac{\partial^2 u}{\partial r^2}\right]$$
$$=\nu\left[\frac{\partial^2 u}{\partial r^2}+\frac{1}{r}\frac{\partial u}{\partial r}\right]-\frac{\sigma B_0^2}{\rho_f}\left(u+\lambda_1 w\frac{\partial u}{\partial r}\right)+\frac{1}{\rho_f}\begin{bmatrix}(1-C_f)\rho_f\beta^{**}g*(T-T_\infty)\\-(\rho_p-\rho_f)g^*(C-C_\infty)\\-(N-N_\infty)g^*\gamma^*(\rho_m-\rho_f)\end{bmatrix}, \tag{2}$$

$$\frac{\partial T}{\partial t}+u\frac{\partial T}{\partial z}+w\frac{\partial T}{\partial r}=\alpha_1\left[\frac{\partial^2 T}{\partial r^2}+\frac{1}{r}\frac{\partial T}{\partial r}\right]+\tau\left[D_B\frac{\partial C}{\partial r}\frac{\partial T}{\partial r}+\frac{D_T}{T_\infty}\left(\frac{\partial T}{\partial r}\right)^2\right]-\frac{1}{(\rho c)_f}\left[\frac{1}{r}\frac{\partial}{\partial r}(rq_r)\right]$$
$$+Q_0\left(\frac{T-T_\infty}{(\rho c)_f}\right), \tag{3}$$

$$\frac{\partial C}{\partial t}+u\frac{\partial C}{\partial z}+w\frac{\partial C}{\partial r}=D_B\frac{1}{r}\frac{\partial}{\partial r}\left[r\frac{\partial C}{\partial r}\right]+\frac{D_T}{T_\infty}\frac{1}{r}\frac{\partial}{\partial r}\left[r\frac{\partial T}{\partial r}\right]$$
$$-Kr^2(C-C_\infty)\left(\frac{T}{T_\infty}\right)^n\exp\left(\frac{-E_a}{kT_\infty}\right), \tag{4}$$

$$\frac{\partial N}{\partial t}+u\frac{\partial N}{\partial z}+w\frac{\partial N}{\partial r}+\frac{bW_c}{(C_w-C_\infty)}\left[\frac{\partial}{\partial r}\left(N\frac{\partial C}{\partial r}\right)\right]=D_m\left(\frac{\partial^2 N}{\partial r^2}\right), \tag{5}$$

with relative boundary conditions:

$$\left.\begin{aligned}&u(t,z,r)=u(t,z)+U_{slip}=\frac{az}{1-\gamma t}+U_{slip},\ w(t,z,r)=0,\\&-k\frac{\partial T}{\partial r}=h_f\left(T_f-T\right),\ D_B\frac{\partial C}{\partial r}+\frac{D_T}{T_\infty}\frac{\partial T}{\partial r}=0, N=N_w,\quad at\quad r=R_1\end{aligned}\right\} \tag{6}$$

$$u\to 0,\ T\to T_\infty,\ C\to C_\infty, N\to N_\infty,\quad as\ \ r\to\infty \tag{7}$$

The slip relations with higher order are:

$$U_{slip}=A\frac{\partial u}{\partial r}+B\frac{\partial^2 u}{\partial r^2}. \tag{8}$$

where u and w represents the velocity components along z axis and r direction, respectively., ν displays the kinematic viscosity, λ_1 is relaxation time parameter, α_1 thermal diffusivity, τ heat capacity ratio, Q_0 heat source /sink, T_∞ be ambient temperature, C_∞ ambient concentration of nanofluid,ρ_f fluid density, β^{**} volume exception coefficient is, g^*gravity, D_B Brownian diffusion coefficient, D_T thermophoresis diffusion coefficient, Kr^2 explains the reaction rate, n is fitted rate constant, b be chemotaxis constant while W_c is the cell swimming speed.

Let us introduce following e appropriate variables [46]:

$$u=\frac{az}{1-\gamma t}f'(\zeta),\ w=\frac{-R_1}{r}\sqrt{\frac{a\nu}{(1-\gamma t)}}f(\zeta),\theta(\zeta)=\frac{T-T_\infty}{T_w-T_\infty},$$
$$\varphi(\zeta)=\frac{C-C_\infty}{C_w-C_\infty},\ \zeta=\sqrt{\frac{a}{\nu(1-\gamma t)}}\left(\frac{r^2-R^2}{2R_1}\right). \tag{9}$$

The reduced system in view of above variables is:

$$(1+2\alpha\zeta)f'''+2\alpha ff''-\frac{S}{2}\zeta f''-Sf'-f'^2+ff''-\frac{7}{4}\beta S^2\zeta f''-\frac{\beta}{4}\zeta^2S^2f'''$$
$$-2\beta S^2f'-2S\beta f'^2-\beta\zeta Sf'f''+3S\beta ff''+S\beta\zeta ff'''+2\beta ff'f''$$
$$-\frac{\alpha\beta}{(1+2\alpha\zeta)}f^2f''-\beta f^2f'''-M^2(f'-\beta ff'')+\lambda(\theta-Nr\varphi-Nc\chi)=0, \tag{10}$$

$$\left(1+\frac{4}{3}Rd\right)(1+2\alpha\zeta)\theta''+\left[\left\{1+Rd(1+(\theta_w-1)\theta)^3\right\}(1+2\alpha\zeta)\theta'\right]\theta''+2\alpha\theta'+Prf\theta'$$
$$-Pr\frac{S}{2}\zeta\theta+(1+2\alpha\zeta)PrNb\theta'\varphi'+(1+2\alpha\zeta)PrNt\theta'^2+Pr\delta\theta=0, \tag{11}$$

Table. 1
Comparison of results when $\alpha = S = 0$.

β	Khan et al. [46]	Abel et al. [47]	Present results
0.0	1.000000	1.000000	1.000000
0.2	1.051866	1.051948	1.051870
0.4	1.101880	1.101850	1.101855
0.6	1.150144	1.150163	1.150146

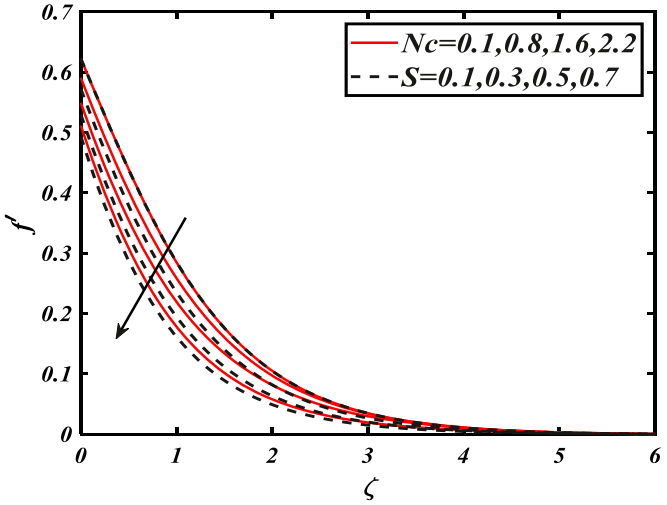

Fig. 2. Variation of $f^{'}$ for Nc and S

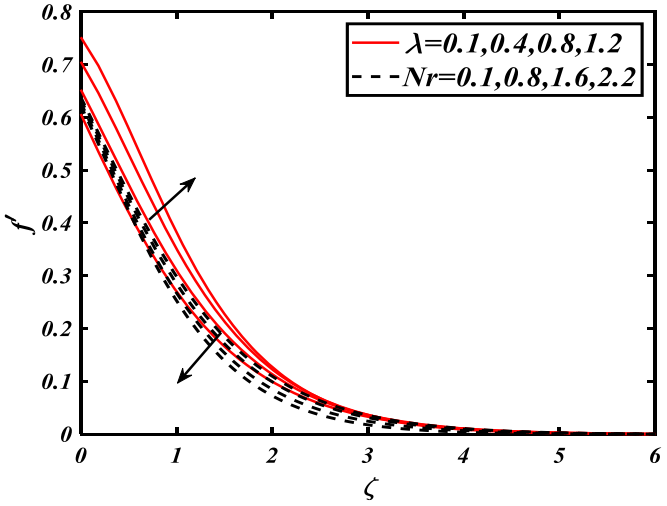

Fig. 3. Variation of $f^{'}$ for λ and Nr

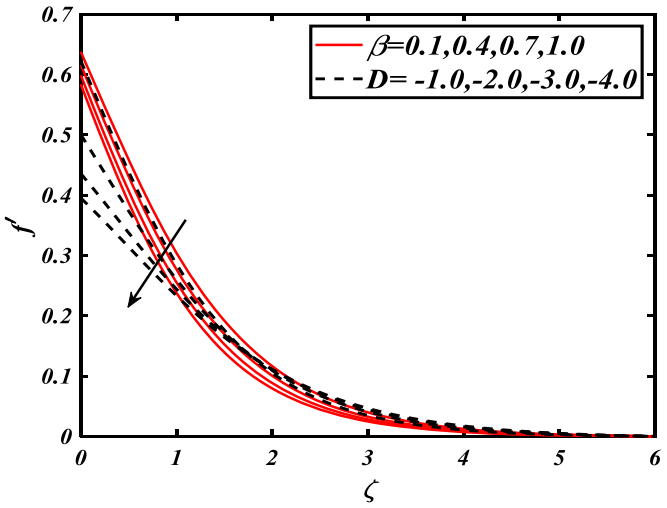

Fig. 4. Variation of $f^{'}$ for β and D

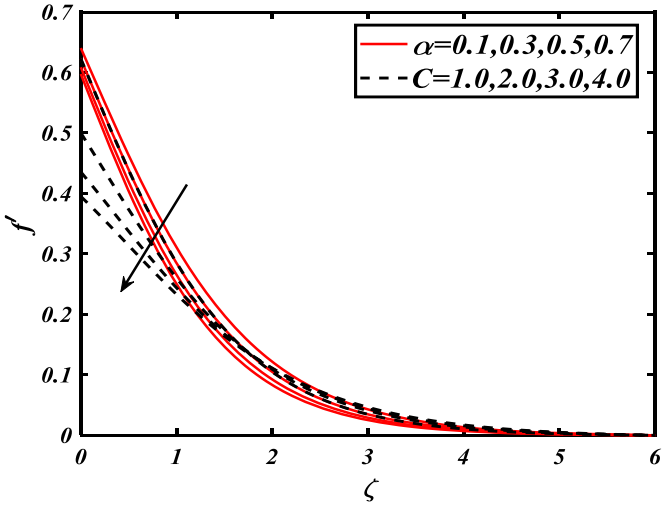

Fig. 5. Variation of $f^{'}$ for α and C

$$(1+2\alpha\zeta)\varphi'' + 2\alpha\varphi' + Le\mathrm{Pr}f\varphi' - LePr\frac{S}{2}\zeta\varphi' + (1+2\alpha\zeta)\frac{Nt}{Nb}\theta'' + 2\alpha\frac{Nt}{Nb}\theta' - Le\mathrm{Pr}\sigma[1+\delta_0\theta]^n\exp\left(\frac{-E}{1+\delta_0\theta}\right)\varphi = 0, \tag{12}$$

$$(1+2\alpha\zeta)\chi'' + 2\alpha\chi' + Le\mathrm{Pr}f\chi' - LePr\frac{S}{2}\zeta\chi' - Pe(\varphi''(\chi+\varpi)+\chi'\varphi') = 0, \tag{13}$$

with dimensionless boundary constraints:

$$\begin{aligned} &f(0)=0, f'(0)=1+Cf''(\zeta)+Df'''(\zeta),\ \theta'(0)=-Bi(1-\theta(0)),\\ &Nb\varphi'(0)+Nt\theta'(0), \chi(0)=1,\\ &f'(\infty)\to 0, \theta(\infty)\to 0, \varphi(\infty)\to 0, \chi(\infty)\to 0 \end{aligned} \tag{14}$$

In which, S designates the unsteady parameter, α stand for curvature parameter, $\beta$is the Maxwell fluid parameter, Pr authorizes the Prandtl number, Nb signify the Brownian motion parameter, Nr express the buoyancy ratio parameter, Nc depicts the bioconvection Rayleigh number, the thermophoresis parameter is symbolized by Nt,Ledenotes the Lewis number, $Rd$the thermal radiation parameter, δ is the heat source/sink parameter, σ indicates the chemical reaction parameter, E for activation energy parameter, δ_0 symbolizes temperature difference parameter, Lb specify the bioconvection Lewis number, Pe stand for Peclet numberand ϖindicates

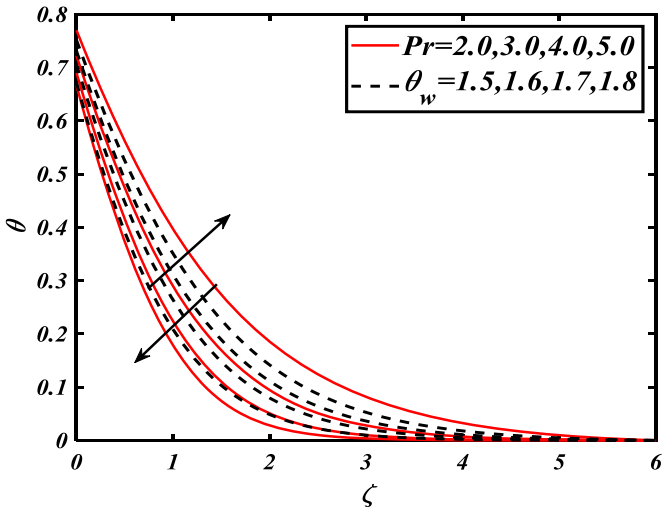

Fig. 6. Variation of θ for Pr and θ_w

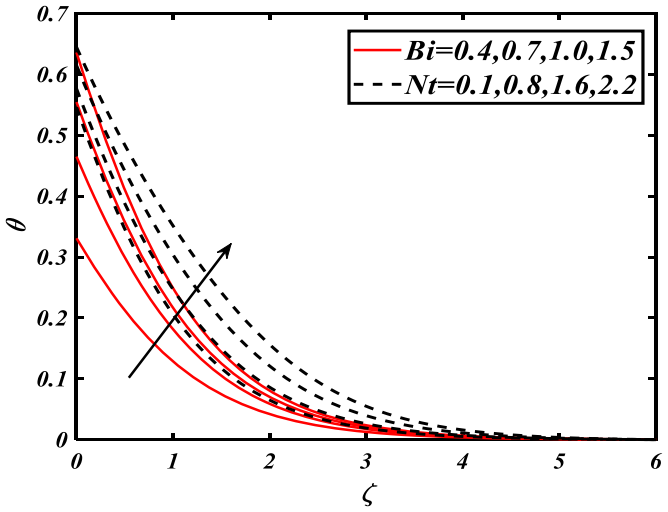

Fig. 7. Variation of θ for Bi and Nt

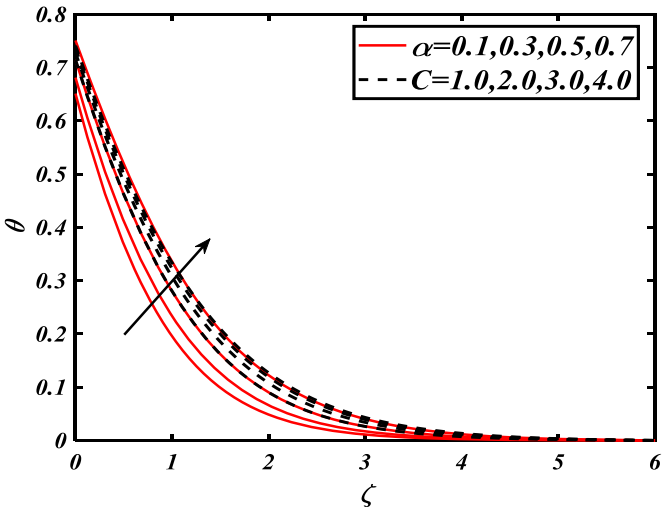

Fig. 8. Variation of θ for α and C

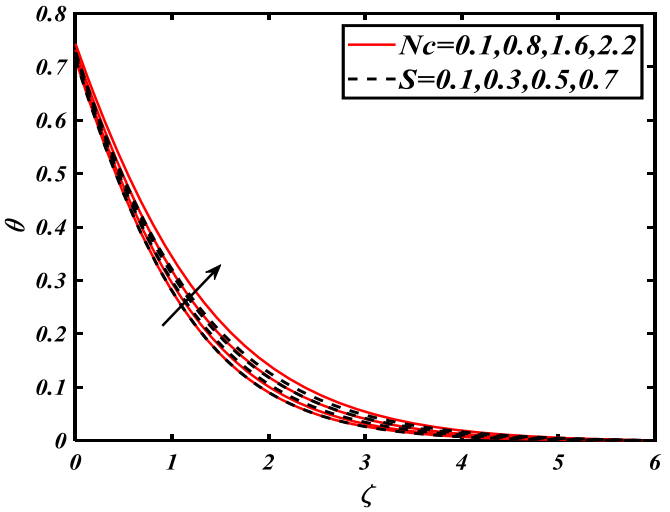

Fig. 9. Variation of θ for Nc and S

microorganism difference parameter, first order velocity slip variable represented by C, second order velocity slip constraints is$D$ and Biot number Biwhich are mathematically represented as follows:

$$\left.\begin{aligned}
&S=\frac{\gamma}{a},\alpha=\frac{1}{R_1}\sqrt{\frac{\nu(1-\gamma t)}{a}},\beta=\frac{\lambda_1 a}{1-\gamma t},M=\sqrt{\frac{\sigma l B_0^2}{U_0\rho_f}},Pr=\frac{\nu}{\alpha_1},Nb=\frac{\tau D_B(C_w-C_\infty)}{\nu},\\
&Nr=\frac{(C_f-C_\infty)(\rho_p-\rho_f)}{\rho_f\beta^{**}(1-C_f)(T_f-T_\infty)},Nc=\frac{\gamma^*(\rho_m-\rho_f)(N_f-N_\infty)}{\rho_f\beta^{**}(1-C_f)(T_f-T_\infty)},Nt=\frac{\tau D_B(T_w-T_\infty)}{\nu T_\infty},\\
&Le=\frac{\alpha_1}{D_B},Rd=\frac{4\sigma^* T_\infty^3}{kk^*},\delta=\frac{Q_0(1-\gamma t)}{a(\rho c)_f},\sigma=\frac{aKr^2}{(1-\gamma t)},E=\frac{E_a}{kT_\infty},\delta_0=\frac{T_w-T_0}{T_\infty},Lb=\frac{\nu}{D_m},\\
&Pe=\frac{bW_c}{D_m},\varpi=\frac{N_\infty}{N_w-N_0},C=A\frac{r}{R_1}\sqrt{\frac{a}{\nu(1-\gamma t)}},D=B\left(\frac{a}{\nu(1-\gamma t)}\right)\frac{r}{R_1},Bi=\frac{h_f}{k}\sqrt{\frac{\nu(1-\gamma t)}{a}}
\end{aligned}\right\} \tag{15}$$

For engineering quantities of interest the Nusselt number, Sherwood number and microorganisms density number can be described as [46]:

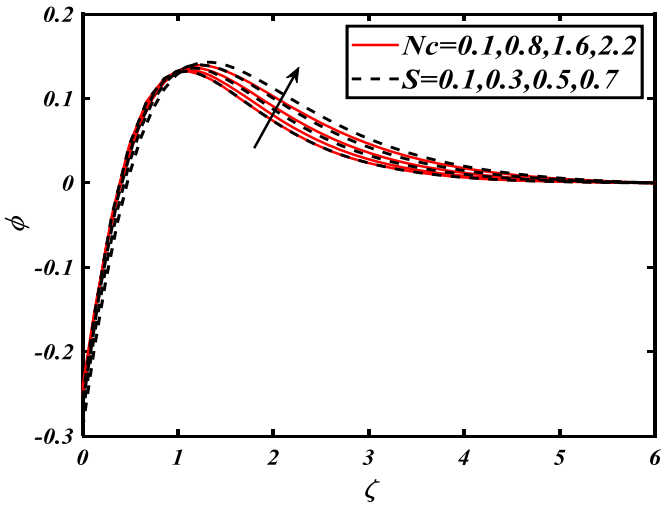

Fig. 10. Variation of φ for Nc and S

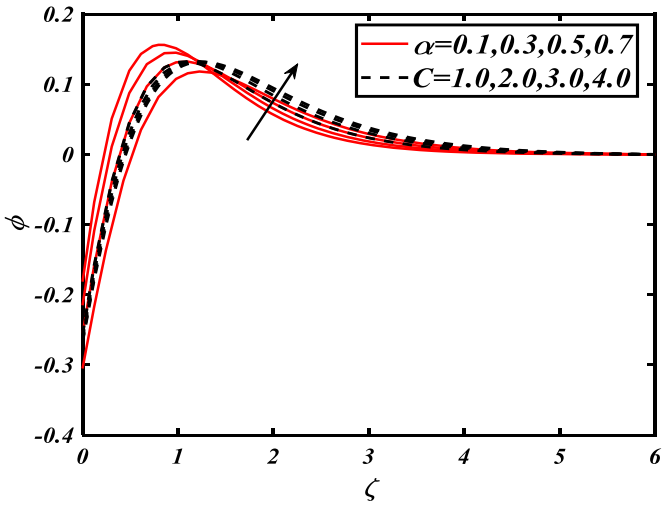

Fig. 11. Variation of φ for α and C

$$\left.\begin{aligned} Nu_z Re_z^{\frac{-1}{2}} &= -\left(1+\frac{4Rd}{3}\right)\theta'(0),\\ Sh_z Re_z^{\frac{-1}{2}} &= -\varphi'(0),\\ Sn_z Re_z^{\frac{-1}{2}} &= -\chi'(0) \end{aligned}\right\} \tag{16}$$

3. Numerical Approach

The modified equations (8-11) with relevant boundary conditions (14) are numerically solved with shooting technique. Following expressions are intorudced to convert the boundary value problem into initial value problem:

$$\left.\begin{aligned} &f = q_1, f' = q_2, f'' = q_3, f''' = q'_3,\\ &\theta = q_4, \theta' = q_5, \theta'' = q'_5,\\ &\varphi = q_6, \varphi' = q_7, \varphi'' = q'_7,\\ &\chi = q_8, \chi' = q_9, \chi'' = q'_9 \end{aligned}\right\} \tag{17}$$

In view of above expressions, Eqs. (8-11) yield:

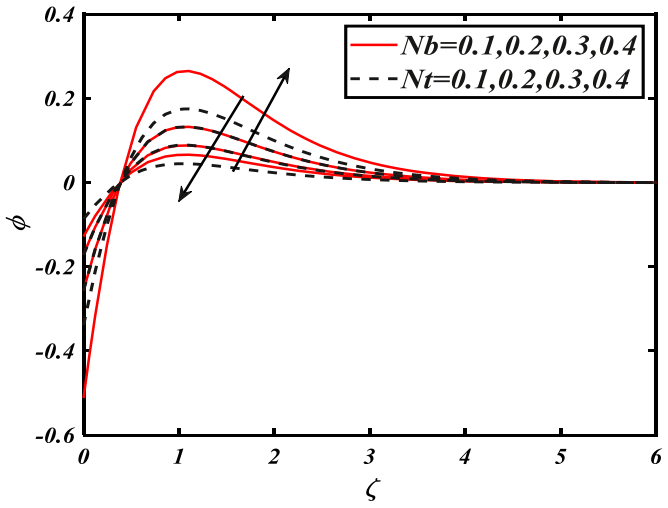

Fig. 12. Variation of φ for *Nb* and *Nt*

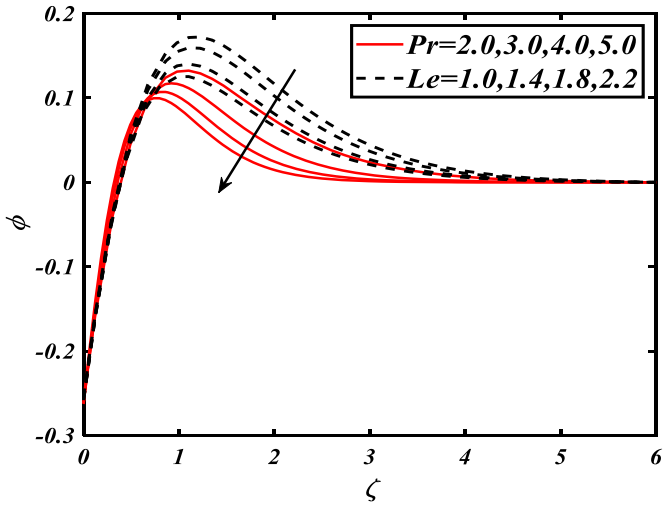

Fig. 13. Variation of φ for *Pr* and *Le*

$$q_3' = \frac{\begin{array}{l} -2\alpha q_1 q_3 + \frac{S}{2}\zeta q_3 + S q_1 + q_2^2 - q_1 q_3 + \frac{7}{4}\beta S^2 \zeta q_3 + 2\beta S^2 q_2 + 2S\beta q_2^2 + \beta\zeta S q_2 q_3 \\ -3S\beta q_1 q_3 - 2\beta q_1 q_2 q_3 + \frac{\alpha\beta}{(1+2\alpha\zeta)} q_1^2 q_3 - \lambda(q_4 - Nrq_6 - Ncq_8) \end{array}}{\left((1+2\alpha\zeta) - \beta q_1^2 - \frac{\beta}{4}\zeta^2 S^2 + S\beta\zeta q_1\right)}, \tag{18}$$

$$q_5' = \frac{-2\alpha q_5 - Pr q_1 q_5 + Pr\frac{S}{2}\zeta q_4 - (1+2\alpha\zeta)\mathrm{Pr}Nbq_5 q_7 - (1+2\alpha\zeta)\mathrm{Pr}Ntq_5^2 - Pr\delta q_4}{\left(1+\frac{4}{3}Rd\right)(1+2\alpha\zeta) + \left[\left\{1+Rd(1+(\theta_w-1)q_4)^3\right\}(1+2\alpha\zeta)q_5\right]}, \tag{19}$$

$$q_7' = \frac{\begin{array}{l} -2\alpha q_7 - LePr\, q_1 q_7 + LePr\frac{S}{2}\zeta q_7 - (1+2\alpha\zeta)\frac{Nt}{Nb}q'_5 - 2\alpha\frac{Nt}{Nb}q_5 \\ +\mathrm{Re}Le\mathrm{Pr}\sigma[1+\delta_0 q_4]^n \exp\left(\frac{-E}{1+\delta_0 q_4}\right) q_6 \end{array}}{(1+2\alpha\zeta)}, \tag{20}$$

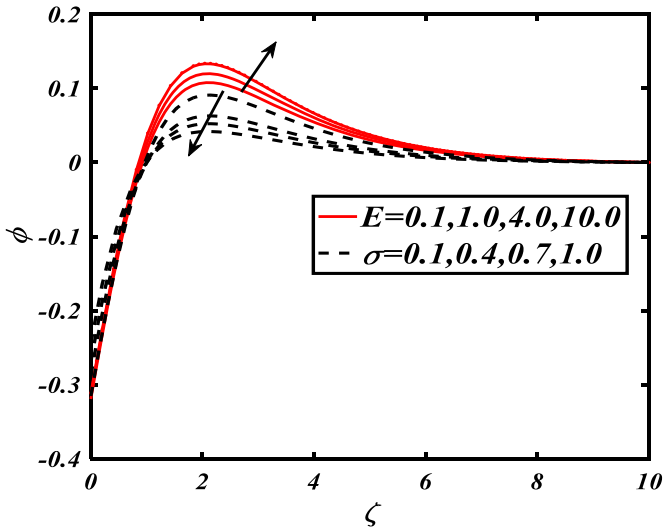

Fig. 14. Variation of φ for E and σ.

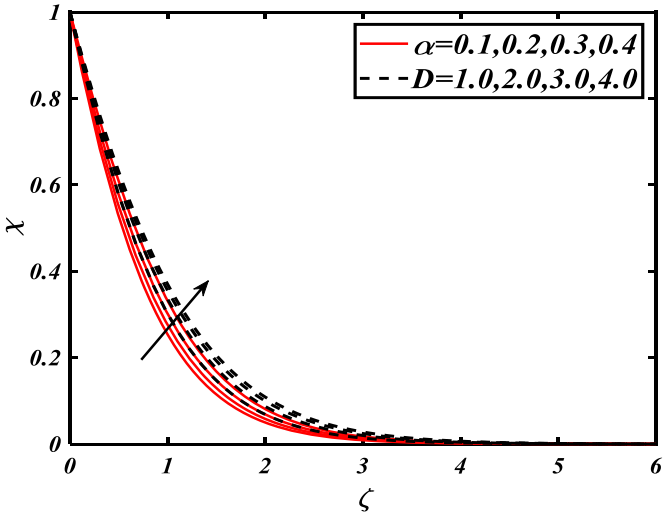

Fig. 15. Variation of χ for α and D

$$q_9^{'} = \frac{-2\alpha q_9 - Le\mathrm{Prq}_1 q_9 + LePr\frac{S}{2}\zeta q_9 + Pe(q^{'}{}_7(q_8+\varpi) + q_9 q_7)}{(1+2\alpha\zeta)}, \tag{21}$$

with

$$\begin{aligned} &q_1(0)=0,\ q_2(0)=1+Cq_3(0)+Dq^{'}{}_3(0),\ q_5(0)=-Bi(1-q_4(0)),\\ &Nbq_7(0)+Ntq_5(0),\ \ q_8(0)=1,\\ &q_2(\infty)=0, q_4(\infty)=0,\ q_6(\infty)=0,\ q_8(\infty)=0. \end{aligned} \tag{22}$$

MATLAB software is used to perform the simulations. All the numerical simulations are performed with accuracy of 10^{-6}.

4. Solution validation

The solution confirmation is done by evaluating the numerical results in table 1 with analysis of Khan et al. [46] and Abel et al. [47]. For limiting case, the obtained numerical simulations shown a very excellent agreement.

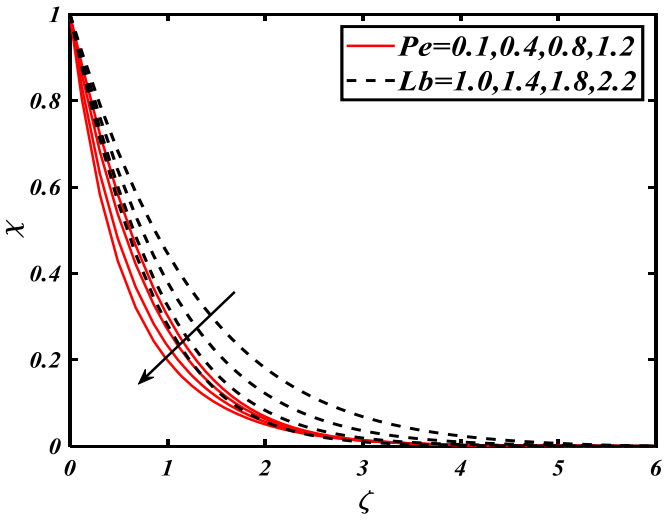

Fig. 16. Variation of χ for *Pe* and *Lb*

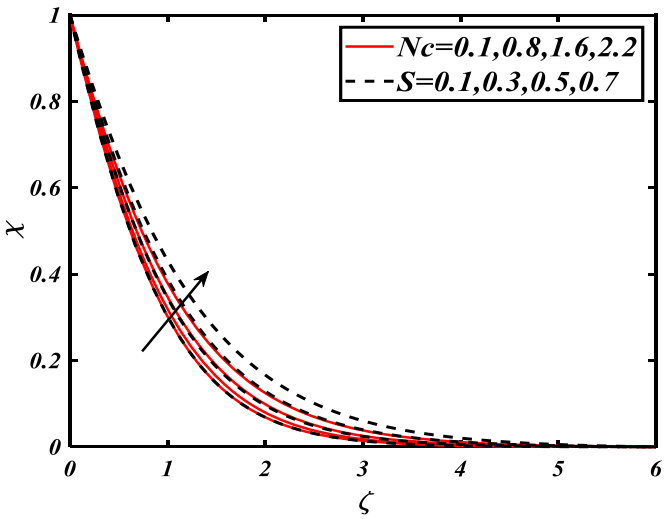

Fig. 17. Variation of χ for *Nc* and *S*

5. Results and discussion

In this section, the physical behavior of various parameters against the velocity, temperature, concentration and microorganism profiles are nanofluid is addressed. Fig. 2 reveals the behavior of bioconvection Rayleigh number *Nc* and unsteadiness parameter *S* on fluid velocity f'. The velocity f' shows a reducing trend for bioconvection Rayleigh number *Nc* and unsteadiness parameter *S*. Physically, the declining change in velocity due to bioconvection Rayleigh number is associated with buoyancy forces. The variation of f' for mixed convection parameter λ and buoyancy ratio parameter *Nr*is captured in Fig. 3. It is seen that fluid velocity rises for larger variation of mixed convection parameter λ. It is further depicted that a reduction in f' is associated to buoyancy ratio parameter *Nr*. To inspect the structure of velocity f' for intensified variation of Maxwell fluid parameter β and second order velocity slip parameter *D*, Fig. 4 is sketched. The observations figured out that the fluid velocity f' diminishes with the increase of β. The higher values of β is associated to the rheological nature of non-Newtonian fluid while smaller value corresponds to viscous material. The higher values ofβenhance the fluid viscosity which report more resistance to the fluid particles due to which velocity decline. The presence of slip parameters also reports a lower nature of velocity. Fig. 5 aims to examine the trends of velocity f' for curvature parameter α and first order velocity slip parameter *C*. It is analyzed that the higher values of curvature parameter α and first order velocity slip parameter *C* provides resistance to the velocity f'.

Fig. 6 examined the features of Prandtl number *Pr* and temperature ratio parameter θ_w for temperature profile θ. One can depict from this figure thermal field θ increase with θ_w while temperature θ reduce for *Pr*. The physical justification for declining change in θ

Table. 2
Computational outcome for local skin friction $-f''(0)$ coefficient for flow parameters.

λ	Nr	Nc	C	β	α	S	$-f''(0)$
0.1	0.5	0.5	1.0	0.5	0.5	0.5	0.3838
0.6							0.2743
1.2							0.1713
0.1	0.2	0.5	1.0	0.5	0.5	0.5	0.3595
	1.0						0.3639
	2.0						0.3701
0.1	0.5	0.1	1.0	0.5	0.5	0.5	0.3632
		1.0					0.3988
		2.0					0.4499
0.1	0.5	0.5	2.0	0.5	0.5	0.5	0.2372
			3.0				0.1782
			4.0				0.1431
0.1	0.5	0.5	1.0	0.1	0.5	0.5	0.3430
				0.6			0.3792
				1.2			0.4012
0.1	0.5	0.5	1.0	0.5	0.1	0.5	0.3481
					0.6		0.3935
					1.2		0.4207
0.1	0.5	0.5	1.0	0.5	0.5	0.2	0.3874
						0.6	0.4790
						1.2	0.5726

Table. 3
Computational outcome for local Nusselt number $-\theta'(0)$ for flow parameters.

λ	Nr	Nc	C	β	α	S	Pr	Nb	Nt	Bi	θ_w	$-\theta'(0)$
0.1	0.5	0.5	1.0	0.5	0.5	0.5	1.2	0.2	0.3	0.6	0.8	0.4052
0.6												0.4416
1.2												0.4696
0.1	0.2	0.5	1.0	0.5	0.5	0.5	1.2	0.2	0.3	0.6	0.8	0.4138
	1.0											0.4098
	2.0											0.4042
0.1	0.5	0.1	1.0	0.5	0.5	0.5	1.2	0.2	0.3	0.6	0.8	0.4132
		1.0										0.4036
		2.0										0.3881
0.1	0.5	0.5	2.0	0.5	0.5	0.5	1.2	0.2	0.3	0.6	0.8	0.4002
			3.0									0.3923
			4.0									0.3872
0.1	0.5	0.5	1.0	0.1	0.5	0.5	1.2	0.2	0.3	0.6	0.8	0.4206
				0.6								0.4064
				1.2								0.3982
0.1	0.5	0.5	1.0	0.5	0.1	0.5	1.2	0.2	0.3	0.6	0.8	0.4166
					0.6							0.6224
					1.2							0.7975
0.1	0.5	0.5	1.0	0.5	0.5	0.2	1.2	0.2	0.3	0.6	0.8	0.4091
						0.6						0.3974
						1.2						0.3987
0.1	0.5	0.5	1.0	0.5	0.5	0.5	2.0	0.2	0.3	0.6	0.8	0.5709
							3.0					0.6311
							4.0					0.6763
0.1	0.5	0.5	1.0	0.5	0.5	0.5	1.2	0.1	0.3	0.6	0.8	0.5044
								0.4				0.5052
								0.8				0.5054
0.1	0.5	0.5	1.0	0.5	0.5	0.5	1.2	0.2	0.1	0.6	0.8	0.5158
									0.4			0.4995
									0.8			0.4777
0.1	0.5	0.5	1.0	0.5	0.5	0.5	1.2	0.2	0.3	0.4	0.8	0.2511
										0.7		0.3437
										1.0		0.4031
0.1	0.5	0.5	1.0	0.5	0.5	0.5	1.2	0.2	0.3	0.6	1.5	0.5895
											1.7	0.4885
											1.2	0.4143

Table. 4
Computational outcome for local Sherwood number $\varphi'(0)$ for flow parameters.

λ	Nr	Nc	C	β	α	S	Pr	Nb	Nt	Bi	Le	$\varphi'(0)$
0.1	0.5	0.5	1.0	0.5	0.5	0.5	1.2	0.2	0.3	0.6	2.0	0.6078
0.6												0.6625
1.2												0.7074
0.1	0.2	0.5	1.0	0.5	0.5	0.5	1.2	0.2	0.3	0.6	2.0	0.6207
	1.0											0.6147
	2.0											0.6063
0.1	0.5	0.1	1.0	0.5	0.5	0.5	1.2	0.2	0.3	0.6	2.0	0.6198
		1.0										0.6054
		2.0										0.5822
0.1	0.5	0.5	2.0	0.5	0.5	0.5	1.2	0.2	0.3	0.6	2.0	0.6003
			3.0									0.5885
			4.0									0.5809
0.1	0.5	0.5	1.0	0.1	0.5	0.5	1.2	0.2	0.3	0.6	2.0	0.6310
				0.6								0.6097
				1.2								0.5972
0.1	0.5	0.5	1.0	0.5	0.1	0.5	1.2	0.2	0.3	0.6	2.0	0.6249
					0.6							0.9336
					1.2							1.1963
0.1	0.5	0.5	1.0	0.5	0.5	0.2	1.2	0.2	0.3	0.6	2.0	0.6137
						0.6						0.5962
						1.2						0.5980
0.1	0.5	0.5	1.0	0.5	0.5	0.5	2.0	0.2	0.3	0.6	2.0	0.8564
							3.0					0.9467
							4.0					1.0145
0.1	0.5	0.5	1.0	0.5	0.5	0.5	1.2	0.1	0.3	0.6	2.0	1.5113
								0.4				0.3739
								0.8				0.1895
0.1	0.5	0.5	1.0	0.5	0.5	0.5	1.2	0.2	0.1	0.6	2.0	0.2579
									0.4			0.9989
									0.8			1.9107
0.1	0.5	0.5	1.0	0.5	0.5	0.5	1.2	0.2	0.3	0.4	2.0	0.3767
										0.7		0.5155
										1.0		0.6046
0.1	0.5	0.5	1.0	0.5	0.5	0.5	1.2	0.2	0.3	0.6	1.2	0.7587
											1.6	0.7580
											2.2	0.7571

due to *Pr* is presented as higher value of Prandtl number reduces the thermal diffusivity. Fig. 7 indicates the impact of Biot number *Bi* and thermophoresis parameter *Nt* on temperature profile θ. Here, the temperature profile θ is boosted by enhancing the Biot number *Bi* and thermophoresis parameter *Nt*. The increasing variation of θ with Biot number is due to the fact that Biot number is related to the coefficient of heat transfer. Moreover the thermophoresis phenomenon is based on the change in temperature due to nanoparticles movement form a heat surface to cold region because of temperature gradient. The migrated pattern improves the temperature. Fig. 8 estimates the variation of temperature profile θ for curvature parameter α and first order velocity slip parameter *C*. The temperature profile θ is improved for larger estimation of curvature parameter α and first order velocity slip parameter *C*. The characteristics of bioconvection Rayleigh number *Nc* and unsteadiness parameter *S* on θ are indicated in Fig. 9. It is analyzed that θ enhanced for larger estimation of bioconvection Rayleigh number *Nc* and unsteadiness parameter *S*. The increasing temperature due *Nc* is physically related to the buoyancy forces. Fig. 10 captures the behavior of bioconvection Rayleigh number *Nc* and unsteadiness parameter *S* on concentration profile φ. It is scrutinized that concentration φ is enlarged for higher estimation of bioconvection Rayleigh number *Nc* and unsteadiness parameter *S*. Fig. 11 visualizes the performance of curvature parameter α and first order velocity slip parameter *C* on φ. Clearly the concentration φ rises for larger estimation of curvature parameter α and first order velocity slip parameter *C*. Fig. 12 designates the consequence of thermophoresis parameter *Nt* and Brownian motion parameter *Nb* on φ. It is noticed that φ enriches for *Nt* while opposite behavior of φ is observed for *Nb*. The declining profile of φ due to *Nb* is clearly observed as *Nb* reflect a revise relation with dimensionless concentration equation. Fig. 13 illustrates the impact of Prandtl number*Pr* and Lewis number *Le* on concentration φ. It is analyzed that φ declines with larger Prandtl number Pr and Lewis number *Le*. The physical consequences of activation energy parameter E and chemical reaction constant σ is presented in Fig. 14. An increasing change in concentration profile is observed for the activation energy parameter. However, the concentration profile reduces with chemical reaction constant σ.

Fig. 15 discloses the effect of curvature parameter α and second order velocity slip parameter *D* on microorganisms profile χ. It is noted that χ improves with curvature parameter α and second order velocity slip parameter *D*. To scrutinize the outcomes of Peclet number *Pe* and bioconvection Lewis number *Lb* on χ,Fig. 16 is portrayed. It is evident that microorganism profile χ declines for *Pe* and *Lb*. The Peclet number is reversely related to the motile diffusivity due to which χ reduces. Fig. 17 is prepared to estimate the physical outcomes of bioconvection Rayleigh number *Nc* and unsteadiness parameter *S* on χ. Here, χ escalates *Nc* and *S*.

The numerical outcomes for skin friction coefficient $-f''(0)$, local Nusselt number $-\theta'(0)$, Sherwood number $\varphi'(0)$ and motile

Table. 5
Computational outcome for local microorganism density number $-\chi'(0)$ for flow parameters.

λ	Nr	Nc	C	β	α	S	Pe	Lb	$-\chi'(0)$
0.1	0.5	0.5	1.0	0.5	0.5	0.5	0.1	2.0	0.9538
0.6									1.0692
1.2									1.1577
0.1	0.2	0.5	1.0	0.5	0.5	0.5	0.1	2.0	0.9816
	1.0								0.9719
	2.0								0.9581
0.1	0.5	0.1	1.0	0.5	0.5	0.5	0.1	2.0	0.9787
		1.0							0.9434
		2.0							0.8864
0.1	0.5	0.5	2.0	0.5	0.5	0.5	0.1	2.0	0.9199
			3.0						0.8849
			4.0						0.8621
0.1	0.5	0.5	1.0	0.1	0.5	0.5	0.1	2.0	1.0020
				0.6					0.9589
				1.2					0.9304
0.1	0.5	0.5	1.0	0.5	0.1	0.5	0.1	2.0	0.8729
					0.6				1.1263
					1.2				1.3691
0.1	0.5	0.5	1.0	0.5	0.5	0.2	0.1	2.0	0.9382
						0.6			0.7735
						1.2			0.5625
0.1	0.5	0.5	1.0	0.5	0.5	0.5	0.2	2.0	1.0418
							0.6		1.2933
							1.2		1.6774
0.1	0.5	0.5	1.0	0.5	0.5	0.5	0.1	1.2	0.7888
								1.6	0.8894
								2.2	1.0215

density number $-\chi'(0)$ are examined in Tables (2-5). Table 2 is designed to analyze the change in $-f''(0)$ for λ, .., Nc, C, β, α and S. Clearly $-f''(0)$ intensified for greater values of Nr, Nc, C, β, α and S while it declines for λ. The numerical values of local Nusselt number $-\theta'(0)$ are calculated for flow parameters like λ,Nr Nc C β α Pr Nb,Nt,Bi, and θ_w in Table 3. It is scrutinized that $-\theta'(0)$ reduces with for Nr, Nc, C and β. Table 4 reveals the variation of local Sherwood number $\varphi'(0)$ for higher values of flow parameters. The local Sherwood number $\varphi'(0)$ rises forλ. The numerical outcomes for local microorganism number $-\chi'(0)$ for λ, Nr, Nc, C, β, α, S, Pe and $Lb$are shown in Table 5. The density number of microorganisms $-\chi'(0)$ enhanced for higher variations of Pe and Lb.

6. Conclusions

The unsteady bioconvection flow of Williamson nanofluid is numerically examined in presence of higher order slip features. The heat and mass transfer pattern in Williamson nanofluid is inspected with applications of nonlinear thermal radiation and activation energy. The shooting technique is employed to follow the solution procedure. The novel outcomes are:

- Ø A reduced velocity profile is resulted with slip parameters and unsteady constant.
- Ø With increasing impact of Biot number and curvature constant, the temperature profile boosted.
- Ø The presence first and second order slip factors enhanced the nanofluid temperature effectively.
- Ø The curvature parameter and radiation constant improves the nanofluid temperature.
- Ø The concentration profile gets more increasing variation with curvature parameter, activation energy while higher values of reaction constant and unsteady parameter reduced the nanofluid concentration.
- Ø A lower change in microorganisms is observed for Peclet number.

Declaration of Competing Interest

The authors declare that they have no known competing financial interests or personal relationships that could have appeared to influence the work reported in this paper.

Acknowledgment

This work was supported by the Natural Science Foundation of Hunan Province (Grant No.: 2018JJ2016), and the Key Laboratory of Key Technologies of Digital Urban-Rural Spatial Planning of Hunan Province (Grant No.: 2018TP1042.

References

[1] S.U.S. Choi, Enhancing Thermal Conductivity of Fluids with Nanoparticles, 231, ASME Publications-Fed, 1995, pp. 99–106.
[2] J. Buongiorno, Convective transport in nanofluids, J. Heat Transf. 28 (2006) 240–250, https://doi.org/10.1115/1.2150834.
[3] K. Venkatadri, S.A. Gaffar, P. Rajarajeswari, V.R. Prasad, O.A. Bég, H. Khan, Melting heat transfer analysis of electrically conducting nanofluid flow over an exponentially shrinking/stretching porous sheet with radiative heat flux under a magnetic field, Heat Transfer Asian Res 49 (8) (2020) 4281–4303, https://doi.org/10.1002/htj.21827.
[4] H. Mondal, S. Bharti, Spectral Quasi-linearization for MHD Nanofluid Stagnation Boundary Layer Flow due to a Stretching/Shrinking Surface, J. Appl. Comput. Mech. 6 (4) (2020) 1058–1068, https://doi.org/10.22055/jacm.2019.30677.1766.
[5] Z. Ying, B. He, L. Su, Y. Kuang, D. He, C. Lin, Convective heat transfer of molten salt-based nanofluid in a receiver tube with non-uniform heat flux, Appl. Therm. Eng. 181 (2020), 115922, https://doi.org/10.1016/j.applthermaleng.2020.115922.
[6] M. Waqas, M.I. Khan, T. Hayat, A. Alsaedi, Stratified flow of an Oldroyd-B nanoliquid with heat generation, Results Phys 7 (2017) 2489–2496, https://doi.org/10.1016/j.rinp.2017.06.030.
[7] M.R. Eid, M.A. Nafe, Thermal conductivity variation and heat generation effects on magneto-hybrid nanofluid flow in a porous medium with slip condition, Waves Random Complex (2020), 10.1080/17455030.2020.1810365 10.1080/17455030.2020.1810365.
[8] W. He, R. Mashayekhi, D. Toghraie, O.A. Akbari, Z. Li, I. Tlili, Hydrothermal performance of nanofluid flow in a sinusoidal double layer microchannel in order to geometric optimization, Int. Commun. Heat and Mass 117 (2020), 104700, https://doi.org/10.1016/j.icheatmasstransfer.2020.104700.
[9] Sami Ullah Khan, Sabir Ali Shehzad, Brownian movement and thermophoretic aspects in third grade nanofluid over oscillatory moving sheet, Physica Scripta 94 (9) (2019), 095202, https://doi.org/10.1088/1402-4896/ab0661.
[10] Sami Ullah Khan, H. Waqas, S.A. Shehzad, M. Imran, Theoretical analysis for tangent hyperbolic nanoparticles with combined electrical MHD, activation energy and Wu's slip features: A mathematical model, Physica Scripta 94 (12) (2019), 125211, https://doi.org/10.1088/1402-4896/ab399f.
[11] S. U.Khan, I. Tlili, H. Waqas, M. Imran, Effects of nonlinear thermal radiation and activation energy on modified second-grade nanofluid with Cattaneo–Christov expressions, J. Therm. Anal. Calorim. 143 (2021) 1175–1186, https://doi.org/10.1007/s10973-020-09392-6.
[12] H. Waqas, M. Imran, S.U. Khan, M.A.Meraj S.A.Shehzad, Slip flow of Maxwell viscoelasticity-based micropolar nanoparticles with porous medium: a numerical study, Appl. Math.Mech. 40 (9) (2019) 1255–1268, https://doi.org/10.1007/s10483-019-2518-9.
[13] M.H.A. Kamal, A. Ali, S. Shafie, N.A. Rawi, R M., Ilias, g-Jitter effect on heat and mass transfer of 3D stagnation point nanofluid flow with heat generation, Ain Shams Eng. J. 11 (4) (2020) 1275–1294, https://doi.org/10.1016/j.asej.2020.03.008.
[14] N. S.Anuar, N. Bachok, N.M. Arifin, H. Rosali, Numerical Solution of Stagnation Point Flow and Heat Transfer over a Nonlinear Stretching/Shrinking Sheet in Hybrid Nanofluid: Stability Analysis, J. Adv. Res. Fluid Mech. Therm. Sci. 76 (2) (2020) 85–98, https://doi.org/10.37934/arfmts.76.2.8598.
[15] R. Rizwana, A. Hussain, S. Nadeem, Slip Effects on Unsteady Oblique Stagnation Point Flow of Nanofluid in a View of Inclined Magnetic Field, Math. Probl. Eng 2020 (2020), 6580409, https://doi.org/10.1155/2020/6580409.
[16] S. S.Giri, K. Das, P.K Kundu, Influence of nanoparticle diameter and interfacial layer on magnetohydrodynamic nanofluid flow with melting heat transfer inside rotating channel, Math. Methods Appl. Sci. 44 (2) (2021) 1161–1175, https://doi.org/10.1002/mma.6818.
[17] B. Mahanthesh, S.A. Shehzad, T. Ambreen, S.U. Khan, Significance of Joule heating and viscous heating on heat transport of MoS2–Ag hybrid nanofluid past an isothermal wedge, J. Therm. Anal. Calorim. 143 (2021) 1221–1229, https://doi.org/10.1007/s10973-020-09578-y.
[18] J. Akram, N.S. Akbar, D. Tripathi, Numerical simulation of Electrokinetically Driven Peristaltic Pumping of Silver-Water Nanofluids in an asymmetric microchannel, Chin, J. Phys. 68 (2020) 745–763, https://doi.org/10.1016/j.cjph.2020.10.015.
[19] D.Tripathi V.K.Narla, O.A. Bég, Electro-osmotic nanofluid flow in a curved microchannel, Chin. J. Phys. 67 (2020) 544–558, https://doi.org/10.1016/j.cjph.2020.08.010.
[20] N. S.Akbar, D. Tripathi, Z. H.t Khan, O.A. Bég, Mathematical model for ciliary-induced transport in MHD flow of Cu-H2O nanofluids with magnetic induction, Chin, J. Phys. 55 (3) (2017) 947–962, https://doi.org/10.1016/j.cjph.2017.03.005.
[21] A. Shahid, Z. Zhou, M.M. Bhatti, D. Tripathi, Magnetohydrodynamics Nanofluid Flow Containing Gyrotactic Microorganisms Propagating Over a Stretching Surface by Successive Taylor Series Linearization Method, Microgravity Sci. Technol. 30 (2018) 445–455, https://doi.org/10.1007/s12217-018-9600-2.
[22] N. S.Akbar, D. Tripathi, Z.H. Khan, Numerical investigation of Cattanneo-Christov heat flux in CNT suspended nanofluid flow over a stretching porous surface with suction and injection, Dis. Cont. Dyn.l Sys. Series S. 11 (4) (2018) 583–594, https://doi.org/10.3934/dcdss.2018033.
[23] N.S.Akbar M.K.Nayak, Z.H.Khan V.S.Pandey, D. Tripathi, 3D free convective MHD flow of nanofluid over permeable linear stretching sheet with thermal radiation, Powder Technol 315 (2017) 205–215, https://doi.org/10.1016/j.powtec.2017.04.017.
[24] S. Arrhenius, Über die Dissociationswärme und den Einfuss der Temperatur auf den Dissociationsgrad der Elektrolyte, Z. Phys.Chem. 4 (1889) 96–116.
[25] A.R. Bestman, Natural convection boundary layer with suction and mass transfer in a porous medium, Int. J. Energy Res. 14 (1990) 389–396, https://doi.org/10.1002/er.4440140403.
[26] M.Arshad T.Salahuddin, N. Siddique, A.S. Alqahtani, M.Y. Malik, Thermophyical properties and internal energy change in Casson fluid flow along with activation energy, Ain Shams Eng. J. 11 (4) (2020) 1355–1365, https://doi.org/10.1016/j.asej.2020.02.011.
[27] M.I. Khan, A.M.El Shafey M.Yousaf, Arrhenius activation energy and Joule heating for Walter-B fluid with Cattaneo–Christov double-diffusion model, J. Therm. Anal. Calorim. 143 (2021) 3687–3698, https://doi.org/10.1007/s10973-020-09270-1.
[28] M. I.Khan, M.W.A. Khan, A. Alsaedi, T. Hayat, M.I. Khan, Entropy generation optimization in flow of non-Newtonian nanomaterial with binary chemical reaction and Arrhenius activation energy, Physica A 38 (2020), 122806, https://doi.org/10.1016/j.physa.2019.122806.
[29] J.R. Platt, Bioconvection patterns' in cultures of free swimming organisms, Science 133 (1961) 1766–1767.
[30] A.V. Kuznetsov, The onset of nanofluid bioconvection in a suspension containing both nanoparticles and gyrotactic microorganisms, Int. Commun. Heat Mass Transfer 37 (2010) 1421–1425, https://doi.org/10.1016/j.icheatmasstransfer.2010.08.015.
[31] A.V. Kuznetsov, Nanofluid bioconvection in water-based suspensions containing nanoparticles and oxytactic microorganisms: oscillatory instability, Nanoscale Res. Lett. 6 (2011) 100, https://doi.org/10.1186/1556-276X-6-100.
[32] Haq F., M. Saleem, M.U. Rahman, Investigation of natural bio-convective flow of Cross nanofluid containing gyrotactic microorganisms subject to activation energy and magnetic field, Phys. Scr. 95 (10) (2020), 105219, https://doi.org/10.1088/1402-4896/abb966.
[33] S. Ahmad, M. Ashraf, K. Ali, Nanofluid Flow Comprising Gyrotactic Microorganisms through a Porous Medium, J. Appl. Fluid Mech. 13 (5) (2020) 1539–1549, https://doi.org/10.2298/TSCI190712332A.
[34] R.Nirmalkumar E.Elanchezhian, M. Balamurugan, K.M.Prabu K.Mohana, A Viloria, Heat and mass transmission of an OldroydB nanofluid flow through a stratified medium with swimming of motile gyrotactic microorganisms and nanoparticles, J. Therm. Anal. Calorim. 141 (2020) 2613–2623, https://doi.org/10.1007/s10973-020-09847-w.
[35] M.M Bhatti,, M. Marin, A. Zeeshan, R. Ellahi, S.I. Abdelsalam, Swimming of Motile Gyrotactic Microorganisms and Nanoparticles in Blood Flow Through Anisotropically Tapered Arteries, Frontiers Phys 8 (2020) 95, https://doi.org/10.3389/fphy.2020.00095.
[36] S.U. Khan, I. Tlili, Significance of activation energy and effective Prandtl number in accelerated flow of Jeffrey nanoparticles with gyrotactic microorganisms, J. Energy Resour. Technol. 142 (11) (2020), 112101, https://doi.org/10.1115/1.4047248.
[37] A. Shafiq, G. Rasool, C.M. Khalique, S. Aslam, Second Grade Bioconvective Nanofluid Flow with Buoyancy Effect and Chemical Reaction, Symmetry 12 (4) (2020) 621, https://doi.org/10.3390/sym12040621.
[38] A.S. Kotnurkar, D.C. Katagi, Bioconvective peristaltic flow of a third-grade nanofluid embodying gyrotactic microorganisms in the presence of Cu-blood nanoparticles with permeable walls, Multidiscip. Model. Mater. Struct. 17 (2) (2021) 293–316, https://doi.org/10.1108/MMMS-02-2020-0025.
[39] S.Z.Alamri T.Muhammad, H. Waqas, R.Ellahi D.Habib, Bioconvection flow of magnetized Carreau nanofluid under the influence of slip over a wedge with motile microorganisms, J. Therm. Anal. Calorim. 143 (2021) 945–957, https://doi.org/10.1007/s10973-020-09580-4.

[40] U Farooq, F.Malik S.Munir, B. Ahmad, D Lu, Aspects of entropy generation for the non-similar three-dimensional bioconvection flow of nanofluids, AIP Adv 10 (7) (2020), 075110, https://doi.org/10.1063/1.5142877.
[41] K. Hosseinzadeh, A.R.Mogharrebi S.Roghani, A. Asadi, M. Waqas, D.D. Ganji, Investigation of cross-fluid flow containing motile gyrotactic microorganisms and nanoparticles over a three-dimensional cylinder, Alex. Eng. J. 59 (5) (2020) 3297–3307, https://doi.org/10.1016/j.aej.2020.04.037.
[42] R.R. Kairi, S. Shaw, S. Roy, S. Raut, Thermosolutal Marangoni Impact on Bioconvection in Suspension of Gyrotactic Microorganisms Over an Inclined Stretching Sheet, J. Heat Transfer. 143 (3) (2021), 031201, https://doi.org/10.1115/1.4048946.
[43] S Shaw, S.e S Motsa, P.s Sibanda, Magnetic field and viscous dissipation effect on bioconvection in a permeable sphere embedded in a porous medium with a nanofluid containing gyrotactic micro-organisms, Heat Tran Asian Res 47 (5) (2018) 718–734, https://doi.org/10.1002/htj.21337.
[44] V.M. Magagula, S. Shaw, R.R. Kairi, Double dispersed bioconvective Casson nanofluid fluid flow over a nonlinear convective stretching sheet in suspension of gyrotactic microorganism, Heat Tran Asian Res 49 (5) (2020) 2449–2471, https://doi.org/10.1002/htj.21730.
[45] S. Shaw, P. Sibanda, A. Sutradhar, P.V.S.N. Murthy, Magnetohydrodynamics and Soret Effects on Bioconvection in a Porous Medium Saturated With a Nanofluid Containing Gyrotactic Microorganisms, J. Heat Transfer. 136 (5) (2014), 052601, https://doi.org/10.1115/1.4026039.
[46] M. Khan, M.Irfan A.Ahmed, J. Ahmed, Analysis of Cattaneo–Christov theory for unsteady flow of Maxwell fluid over stretching cylinder, J. Therm. Anal. Calorim. 144 (2021) 145–154, https://doi.org/10.1007/s10973-020-09343-1.
[47] M.S. Abel, J.V. Tawade, M.M. Nandeppanavar, MHD flow and heat transfer for the upper-convected Maxwell fluid over a stretching sheet, Meccanica 47 (2012) 385–393, https://doi.org/10.1007/s11012-011-9448-7.